Conductive Block Copolymer Elastomers and Psychophysical Thresholding for Accurate Haptic Effects

Authors: Rachel Blau¹†, Abdulhameed Abdal²†, Nicholas Root⁴, Alexander X. Chen¹, Tarek Rafeedi¹, Robert Ramji¹, Yi Qie¹, Taewoo Kim¹, Anthony Navarro¹, Jason Chin¹, Laura L. Becerra³, Samuel Edmunds³, Samantha M. Russman³, Shadi A. Dayeh³, David P. Fenning¹, Romke Rouw⁴, Darren J. Lipomi¹*

Affiliations:

¹Department of Nano and Chemical Engineering, University of California; San Diego, La Jolla, CA, USA.

²Department of Mechanical and Aerospace Engineering, University of California; San Diego, La Jolla, CA, USA.

³Department of Electrical and Computer Engineering, University of California; San Diego, La Jolla, CA, USA.

⁴Brain and Cognition, Psychology Department, University of Amsterdam; Amsterdam, Netherlands.

*Corresponding author: <u>dlipomi@ucsd.edu</u> (D.J.L)

†These authors contributed equally to this work

20

5

10

15

25

30

35

40

Abstract

5

10

15

Electrotactile stimulus is a form of sensory substitution in which an electrical signal is perceived as a mechanical sensation. The electrotactile effect could, in principle, recapitulate a range of tactile experience by selective activation of nerve endings. However, the method has been plagued by inconsistency, galvanic reactions, pain and desensitization, and unwanted stimulation of non-tactile nerves. Here, we describe how a soft conductive block copolymer, a stretchable layout, and concentric electrodes, along with psychophysical thresholding, can circumvent these shortcomings. These purpose-designed materials, device layouts, and calibration techniques make it possible to generate accurate and reproducible sensations across a cohort of 10 human participants, and to do so at ultra-low currents (≥ 6 microamperes), without pain or desensitization. This material, form factor, and psychophysical approach could be useful for haptic devices and as a tool for activation of the peripheral nervous system.

One Sentence Summary: Tactile stimulation using conductive polymer can be "tuned" to simulate pressure or vibration at low current.

Introduction

5

10

15

20

25

30

35

40

45

The most common haptic effects one encounters in consumer devices are produced by mechanical actuators. The primary function of such devices is to deform the skin to produce various tactile cues, such as, buzz, rumble, and click. Although the sensations produced using these methods are compelling and reproducible, the gamut is highly limited. Ideally, haptic feedback for human-machine interfaces—for example, for education, entertainment, healthcare, and medical devices—should be able to produce a much wider range of tactile cues (I-4). Indeed, haptics have become indispensable for consumer devices, such as, "vibration mode" on a phone. Similarly, patient engagement and usability devices envisioned for stretchable, epidermal sensors could be substantially deepened with this type of unobtrusive cue. Moreover, use cases for epidermal appliances in physical therapy, robot-assisted surgery, and remote operation could be expanded if they could provide haptic feedback.

All tactile sensations which are ultimately perceived by the brain originate as action potentials in afferents of the peripheral nervous system. Thus, it is in principle possible to generate any tactile percept by activating the relevant set of mechanosensory neurons. Transcutaneous electrical stimulation of the mechanoreceptors using electrodes pressed to the skin has thus held promise for many decades, for applications such as haptics, pain relief, and neuroprostheses (5). This electrotactile effect is thus a form of "sensory substitution," in which electrical signals can be perceived as mechanical forces (6). However, electrotactile stimulation as a means of generating haptic effects has been criticized for many reasons (7). It is non-selective, meaning that it produces a range of sensations which are inconsistent between users. This inconsistency owes to differences in skin morphology, unequal hydration, and other parameters which affect contact impedance with the electrodes (8). Moreover, high currents and voltages required when using conventional materials (such as metals) and device layouts (like hard planar substrates) also lead to unwanted effects, such as galvanic reactions at the skin surface, pain, and temporary desensitization (9). Also, the area of stimulation tends to be large, and electrical signals also have the potential to stimulate the muscles as well as the mechanosensors (10).

Nevertheless, the toolkits of materials chemistry, microfabrication engineering, and signal detection theory applied to cognitive science have the potential to increase the realism, safety, and reliability of electrotactile effects (11). Such development would greatly enable haptic effects in epidermal circuits, where devices in wearable form factors would otherwise have to be made thicker to accommodate components with moving parts (12–15). In this article, we use an integrated materials design strategy that combines a purpose-synthesized, stretchable, conductive block copolymer, concentric electrodes in a stretchable layout, and a psychophysical design strategy for consistent stimulation of mechanical sensations in human participants (8, 16, 17). Using these tools and a large data set, we were able to show extraordinarily low stimulation currents (\geq 6 μ A), improved spatial localization, greater acuity by the participant, and the ability to toggle between sensations characterized as pressure versus vibration by modifying the frequency of the signal.

Results

Synthesis of intrinsically stretchable PEDOT-based one-component electrode

Our strategy is illustrated in **Fig. 1**. The material (**Fig. 1A**) is a conductive block copolymer based on the well-known polyelectrolyte complex, poly(3,4-ethylenedioxythiophene):poly(styrenesulfonate) (PEDOT:PSS). To circumvent the stiffness and brittleness of pristine PEDOT:PSS, which does not make conformal coverage with the uneven

surface of the skin, we used a block copolymerization strategy described recently by our group (18, 19). The goal was to make a low-impedance conductive polymer with a high degree of mechanical deformability, and which can be patterned easily into conductive traces. Briefly, a flexible bottlebrush segment based on poly(poly(ethylene glycol) methyl ether acrylate) (PPEGMEA) was covalently bound to the PSS chain using the reversible addition-fragmentation transfer (RAFT) process, a type of quasi-living controlled radical polymerization. The resulting polymer was termed PEDOT:PSS₍₁₎-b-PPEGMEA₍₆₎ ("Block-6"), where the subscripts refer to the mass ratios of the two segments (**figs. S1** to **S5**). Inclusion of the large, flexible units resulted in a much lower elastic modulus than PEDOT:PSS (~10 MPa compared to ~380 MPa) (18). A molecular dynamics simulation of a single polymer chain with associated PEDOT (**Fig. 1B**) revealed the flexible PPEGMEA chains surrounding the stiffer PEDOT:PSS core, reminiscent of common thermoplastic block copolymer elastomers, such as poly(styrene-butadiene-styrene) (SBS). The low elastic modulus of Block-6 allowed for notably greater conformal contact on the surface of the skin (**Fig. 1C** and **fig. S6**). Poor contact leads to increased impedance, larger currents, and greater chance of pain upon stimulation (20, 21).

Electrode design and fabrication

5

10

15

20

25

30

35

40

45

Using laser ablation, we fabricated a design consisting of concentric electrodes in a serpentine layout (**Figs. 1D** and **1E**). Although the addition of serpentine microstructures may not be groundbreaking, it's important to acknowledge that integrating them into our intrinsically stretchable material offers notable advantages. Our material inherently stretched up to approximately 10% elastically, and the incorporation of serpentine microstructures extended its stretchability, making it suitable for use as a skin interface. The details of fabrication are given in (**figs. S7-10**). Briefly, the Block-6 electrodes were deposited atop a thin film of poly(methyl methacrylate) (PMMA) on a stretchable substrate, polydimethylsiloxane (PDMS). We chose to test for tactile effects on the forearm because it represented a greater challenge for controlled tactile effects compared to the fingers, which have a lower stimulation threshold and higher afferent density (22–24).

Recent studies indicate that a range of current densities (0.1 – 10 mA cm⁻²) can stimulate sensory fibers residing at the epidermis-dermis junction (7). In addition, the distribution of the low current density should be localized, to activate nearby mechanoreceptors (and not muscles). Thus, to stimulate locally, a concentric design was adopted for the ventral forearm (Fig. 1E and F and figs. S11 and S12). Finite element analysis (FEA) simulation showed that the current density distribution was localized across the skin layers as opposed to monopolar designs under similar area ($\sim 10 \text{ cm}^2$) and current source ($10 \mu A$) (Fig. 1G and figs. S13). The electrode dimensions were optimized to fit the forearm and the current applied is the average detection threshold from the participants (~10 µA) (fig. S13). The electronic properties utilized for current density simulations are shown in fig. S14 and Table S1. Importantly, we assessed the effectiveness of current density distribution on an embedded nerve fiber in the epidermis layer by implementing the Hodgkin-Huxley model, which describes action potential propagation (Table S2). Schematics illustrating the nerve fiber location and embedment in the dermis are shown in fig. S15 and fig. S16. The model suggests that the action potential only propagates along the fiber when a concentric design is placed on the skin, as it remains untriggered in a conventional electrode due to the non-localized current spread (Fig. 1H and fig. S17). Furthermore, we conducted an evaluation of the dual electrode with a comparable total contact size (505 mm²) to serpentine concentric (509 mm²) and gap distances of 20 mm and 9 mm, as depicted in fig S.13. This assessment revealed an increase in current density compared to the larger dual electrode, and it indeed triggered an action potential

at a 9 mm gap distance (**fig S.18**). However, the gap distance is usually 20 - 50 mm for dual electrodes (25). It is essential to note that existing reports generally favor the use of larger electrodes to minimize the likelihood of inducing painful sensations (26)Consequently, the geometric shape employed influences the magnitude of the current stimulation and the subsequent sensation.

Characterization of Block-6 as a haptic interface

5

10

15

20

25

30

35

40

45

The electrochemical characteristics of the Block-6 electrode influence how charge is transported across the electrode/skin junction. For example, the capacitance of the electric double layer (EDL) within a conductive polymer determines the amount of charge that can be injected (27, 28). PEDOT:PSS exhibited capacitive behavior due to the charged sulfonate groups; these charges permit mixed (ionic and electronic) conductivity (Fig. 2A and fig. S19A) (29). The cyclic voltammetry (CV) of Block-6 showed capacitive behavior by the rectangular shape hysteresis in the voltammogram, and the linear dependence of the current with the scan rate (fig. S19B) (30). In addition, the electronic function of the electrode is dependent on both the electrical and ionic conductivity of Block-6. Although the electrical conductivity of Block-6 is lower than that of pristine PEDOT:PSS, the PPEGMEA chains promote ionic transport, and thus resulted in a greater EDL capacitance, indicated by a greater slope when measured from CV (fig. S19B) (29, 30). The CV additionally exhibited a larger area compared to pristine PEDOT:PSS, suggesting a larger charge storage capacity of Block-6 (Fig. 2B and fig. S20). Finally, the excursion potential of Block-6 and pristine PEDOT:PSS were measured with a charge injection of 2.08 mA mm⁻², and both electrodes showed comparable stability in terms of voltage build-up (Fig. 2C). This is important for safety consideration during charge injection (31). However, increasing the injection current resulted in delamination of PEDOT:PSS (fig. S21), whereas the injection current of the Block-6 electrode could be increased to 36 mA (75 mA cm⁻²) while remaining intact. A critical consideration for wearable electrodes is compatibility with elastic human skin (32). Delamination due to mismatch in modulus can result in increased impedance, increased voltage required for simulation, and greater chance of pain, galvanic reactions, and other unwanted effects. The viscoelasticity of Block-6 permits the local conformability to the uneven surface of the skin, and also lateral stretching due to global deformation of the skin (Fig. 2D, fig. S22). Microscopic conformability in particular is unfeasible for high-modulus metallic films (33). Here, the concentric Block-6 electrodes were designed to have serpentine structures to accommodate increased elastic strain and reduced changes in interfacial impedance upon stretching (Fig. 2E). In addition, impedance measurements on human skin were lower for Block-6 across all frequency ranges (fig. S23). Mechanical simulations suggested that the elasticity of the freestanding Block-6 electrode to be ~44% (fig. S24 and fig. S25). Although the elasticity of the assembled device decreased to ~19% due to the bonded contacts on the elastomeric substrate (fig. S26), this still remains a ~3× improvement compared to recent reports of metallic interconnects on elastomers (34). Likewise, strain-resistance measurements indicated that the Block-6 electrodes exhibited negligible piezoresistivity— meaning no increase in resistance up to 30% for at least 500 cycles (fig. S27). Also, we characterized the contact resistance between silver for Block-6 (0.217 Ohm·cm²), which is comparable to pristine PEDOT: PSS (0.237 Ohm·cm²) (fig. S28). Additionally, simulations suggest that torsion of the electrodes up to 180° results in von-Mises stresses that are less than half of the yield strength (Fig. 2G). Finally, the intrinsic stretchability of the polymer coupled with the serpentine design allows the device to achieve strains of 100% before failure (Fig. 2F). The PPEGMEA chains render a lower loss and storage modulus (Fig. 2H and fig. S29), with higher viscoelasticity than that of pristine PEDOT:PSS (fig. S29 and S30). When

compared to physical blends involving PEDOT (Fig. 2I), the covalently engineered Block-6 possesses the lowest modulus, indicating it is closest to that of human skin.

Psychophysical thresholding for electrotactile perception

5

10

15

20

25

30

35

40

45

Both electrical and mechanical stimuli can activate nerve fibers that evoke the sense of touch. Mechanical stimulus results in the deformation of mechanoreceptors, whereas electrical signals produce a potential gradient across nerve fibers, resulting in depolarization and repolarization events across the membrane of receptor cells. As a result, these stimuli trigger action potentials that ascend towards the central nervous system (CNS) in the same biological pathway (**Fig. 3A**) (35, 36). For mechanical stimulus, the type and intensity of the sensation triggered by activation of mechanoreceptors is a function of displacement and frequency. For example, afferents terminating in the Merkel cell–neurite complexes (slow-adapting type I) are responsible for the sensation of sustained pressure, whereas rapid-adapting mechanoreceptors (RAMs) are sensitive to vibrotactile stimulation (37, 38). A β -fiber RAMs in the hairy skin are tuned to very similar frequencies as those terminating in Meissner corpuscles (rapid-adapting type I) deliver low vibration sensations and are believed to make up part of the sensation of fine textures.

To relate the parameters of electrical stimulation to the sensation perceived, we performed psychophysical experiments on a group of participants (Fig. 3B). Safety protocols were assessed before experimenting with stimulation (fig. S31 and S32). We designed a set of psychophysical tests that will characterize key elements in electrotactile stimulation, including pain and detection thresholds, perception quality, spatial acuity, and contrast discrimination. Detailed psychophysical tasks and procedures are described in fig. \$33 to \$35. Furthermore, we have demonstrated that materials like pristine PEDOT: PSS (known for rigidity) and copper (characterized by high impedance) are impractical for electrotactile applications (fig. S36 and fig. S37). The psychophysical evaluations began with pain threshold measurement by applying biphasic current stimulation ($10 - 250 \mu A$). Measuring pain thresholds enables us to know if a participant might feel noxious on subsequent tasks. Fortunately, the highest intended stimulation current for the detection threshold experiment was ~4× lower than the lowest pain threshold of any participant (Fig. 3C). To quantify the detection threshold associated with the haptic sensations invoked, we used a 2-alternative forced choice (2AFC) design to measure the accuracy with which participants could identify which of two electrotactile devices had been stimulated. Even at the lowest stimulation current of 6 µA, participants' accuracy was notable, reaching 84%, which was significantly higher than would be expected by chance (p < 0.005; see Statistical Analysis), and higher than the 75% accuracy criterion classically used to define the sensory detection threshold (Fig. 3D and fig. S38) (39). To our knowledge, $\leq 6 \mu A$ is among the lowest sensory detection threshold reported for an epidermal electrotactile device.

Evaluation of the quality percept

Idiosyncrasies of the participants, such as differences in skin morphology, hydration, and concentration—can lead to individual differences in sensation (10). In subsequent experiments, we accounted for these individual differences by applying a current amplitude equal to (1T), twice (2T) or three times (3T) the detection threshold level for each participant (rather than applying fixed currents across participants). We hypothesized a gamut of percepts by normalizing the stimulation frequency. Across all combinations of frequency and current of electrical stimulation, participants predominantly experienced the sensation of either pressure or vibration. In fewer than 5% of trials, a different sensation was reported (typically itch, possibly due to the activation of pruriceptors (40). Overall, the participants were significantly more likely to experience vibration

at higher frequencies of stimulation, and pressure at lower frequencies of stimulation (p < 0.001) (Fig. 4A and fig. S39) (41). On average, increasing the stimulation frequency by 70% doubled the odds of experiencing vibration versus pressure. Our model predicts that the "crossover" point at which participants first begin to report vibration more often than pressure is \sim 6 Hz (Fig. 4B). Interestingly, the frequency of the crossover point happens to correspond to the frequency at which Meissner corpuscles (sensitive to low-frequency vibrations) become more sensitive to vibration than Merkel cell-neurite complexes (which typically respond to sustained pressure, but are also sensitive to very low-frequency vibrations) (11, 42). A β -fiber RAMs in hairy skin are sensitive to frequencies between 10 and 50 Hz, similar to the range that activates fibers terminated in Meissner corpuscles found in glabrous skin. This observation suggests that the change in conscious sensation from pressure to vibration might reflect an equivalence (in the elicited patterns of neuronal activation) between electric stimulation and mechanical stimulation at a given frequency (Fig. 4C).

Although the type of sensation (pressure versus vibration) was strongly dependent on the frequency, it was not significantly affected by the current (p > 0.05). Instead, changes in stimulation current affected the intensity of the sensation perceived, with stronger currents corresponding to a more intense sensation (for instance, doubling the stimulation current increased the perceived intensity by approximately 0.25 on the 1-5 intensity scale, **fig. S40**). Importantly, as predicted by the pain thresholding, all sensations were reported to be between "very comfortable" and "neutral" except for a single trial for a single participant (who rated the 10 Hz stimulation at detection threshold as "uncomfortable"). Furthermore, almost all sensations (93%) were experienced as localized rather than referred (5%) or radiating (1%). The probability of experiencing a sensation as localized did not significantly depend on frequency or current (both p > 0.05; **Fig. 4D**). Moreover, we have assembled a comprehensive table for comparing our work to the existing literature (**Table S3**).

Spatial acuity and contrast discrimination

5

10

15

20

25

30

35

40

45

Finally, the types of sensation, spatial acuity, and contrast discrimination achievable by electrotactile means will depend on the type and density of nerve endings found on various regions of the body. Previous studies suggest that the spatial acuity for the forearm by electrical stimulus (a type of two-point discrimination test) is 9-40 mm (7, 43, 44). Using our materials, we varied the inter-electrode distance between two electrodes from 2-10 cm (fig. S41). The smallest distance between electrodes tested was constrained by the outer terminal of the concentric electrode, which had a radius of $\sim 1 \text{ cm}$ (fig. S11 and S12). Even at the smallest possible center-to-center distance, 2 cm, participants could identify whether stimulation came from one versus both electrodes with 95% accuracy (p < 0.001; fig. S42). Overall, the identification of spatial acuity was significantly higher than chance (p < 0.001). There was not a significant relationship between inter-electrode distance and acuity accuracy (p = 0.53). However, increasing the difference in current between the electrodes at a fixed position (meaning the just noticeable difference) corresponded to better accuracy (p < 0.001) (Fig. 4E). On average, increasing the "contrast" in signal by 13% doubled the odds of identifying which site had higher current.

We conducted a comparative analysis of our Block-6 psychophysical results with silver/silver chloride (Ag/AgCl) commercially available electrodes with identical experimental settings (**fig. S43A**). Hence, it is possible to directly compare the electrodes at different amounts of current delivery. The detection performance at 6 μ A was far lower than the accuracy criterion (**fig. S43B**). Therefore, we increased the current amplitude up to 80 μ A for further investigation of the detection threshold (**fig. S43C**). We found that Block-6 outperforms the commercial electrode and the minimum current for above chance performance on the commercial electrode is ~25 μ A (~3x

higher current than with Block-6). Also, the commercial electrode crosses the traditional psychophysics threshold definition of 75% accuracy at ~40 μ A (~5x higher current than with ours). Moreover, the frequency modulation resulted in more thermal and itching sensations (**fig. S43D**). The toggling effect between pressure and vibration was imperceptible with this type of electrode. Lastly, the dual electrode experiences more current spread and thus the response proportion was not localized at all frequencies (**fig. S43E**).

Discussion

5

10

15

20

25

30

35

The generation of haptic effects by direct electrical stimulation of afferent fibers has always held promise as a means of sensory substitution. Here, we have shown how an integrated strategy that includes polymer engineering, device layout, and psychophysical thresholding based on signal detection theory can be used to overcome the occurrence of pain, desensitization, lack of realism, and participant-to-participant variation which has previously hindered this technique. These methods allow delivery of ultralow stimulation currents with high spatial precision. We also demonstrated the ability to "toggle" between sensations categorized by participants as pressure and those categorized by participants as vibration, by adjusting the frequency of electrical stimulation. Moreover, the crossover point in electrical frequency at which perception of vibration is more likely than perception of pressure is similar to the mechanical frequency at which A β -fiber RAMs, a subset of low-threshold mechanoreceptor activated by low-frequency vibrations, become more sensitive than Merkel afferents. This observation suggests an equivalency between electrical and mechanical stimulation. The ability to bypass the mechanically sensitive apparatus and activate the appropriate neurons transcutaneously could be valuable not only in haptics but also in neural prostheses.

We note that several observations in this study may open new avenues for research. For example, our results hinted at the possibility of a type of "tactile contrast": increased discrimination when different electrical signals were supplied by adjacent electrodes. This capability could be highly valuable in the development of tactile displays, human-machine interfaces, accessibility devices, or new forms of artwork, especially for the blind. Furthermore, the results from our cohort in which participants categorized (a small number of) electrotactile stimuli as "itch" or "heat" (in addition to the dominant categories of pressure and vibration) suggest a broader gamut of tactile percepts to the electrotactile effect than may have been previously known. Such results also hint at the ability to achieve multimodal stimulation given a more complex waveform or juxtaposition of electrodes providing different signals.

Finally, we note that the technical sophistication of our electrode setup is not the best that can possibly be achieved. Excellent work of many investigators in the field of epidermal electronics have demonstrated stretchable layouts with greater resolution than those reported here. More sophisticated layouts with multiplexed outputs and tighter resolution—combined with the materials and psychophysical calibration reported here—may still lead to new capabilities.

Figures

5

10

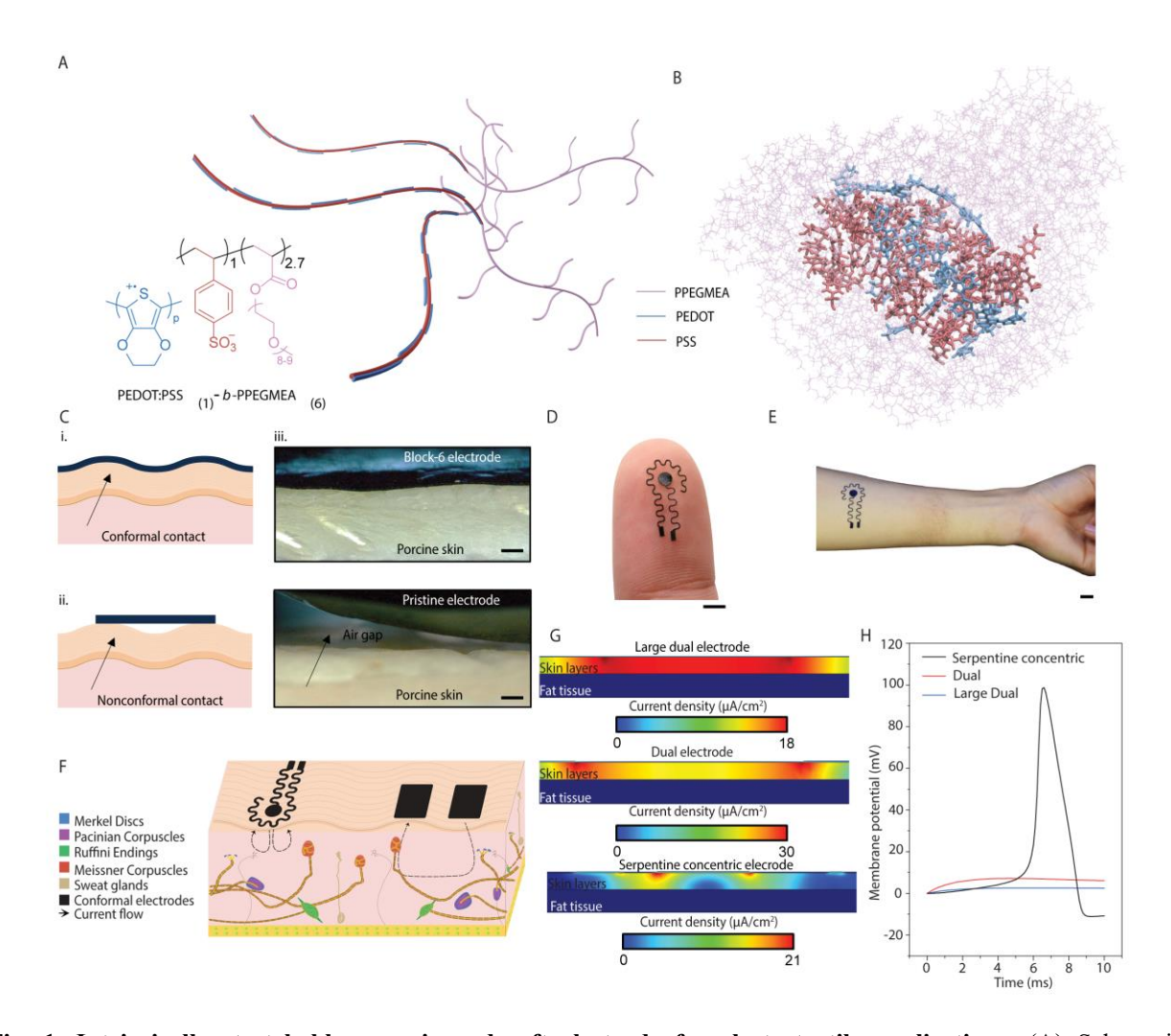


Fig. 1. Intrinsically stretchable organic and soft electrode for electrotactile applications. (A) Schematic illustration of intrinsically stretchable PEDOT derivative known as Block-6. (B) Atomistic molecular dynamics simulation of Block-6. (C) Schematic illustration of (i) Block-6 and (ii) pristine PEDOT:PSS conformability on corrugated skin (iii) High-resolution optical images displaying conformability of the electrode on porcine skin at 200X magnification . Scale bar, 100 μm. (**D** and **E**) Photographic images of conformal and stretchable concentric electrodes on human skin for electrotactile applications, including the fingertip (**D**) and the forearm (**E**). Scale bars of 1 mm and 1 cm, respectively. (**F**) Schematic illustration showing the comparison of current flow in serpentine concentric and dual electrode designs. (**G**) Simulation results of current density distribution in dual and serpentine concentric electrodes. Large electrode has a contact area of 2217 mm². Dual and serpentine electrodes have comparable contact areas of 505 mm² and 509 mm², respectively. (**H**) Hodgkin-Huxley model shows nerve actional potential triggered in serpentine concentric electrode design as a result of localized current density.

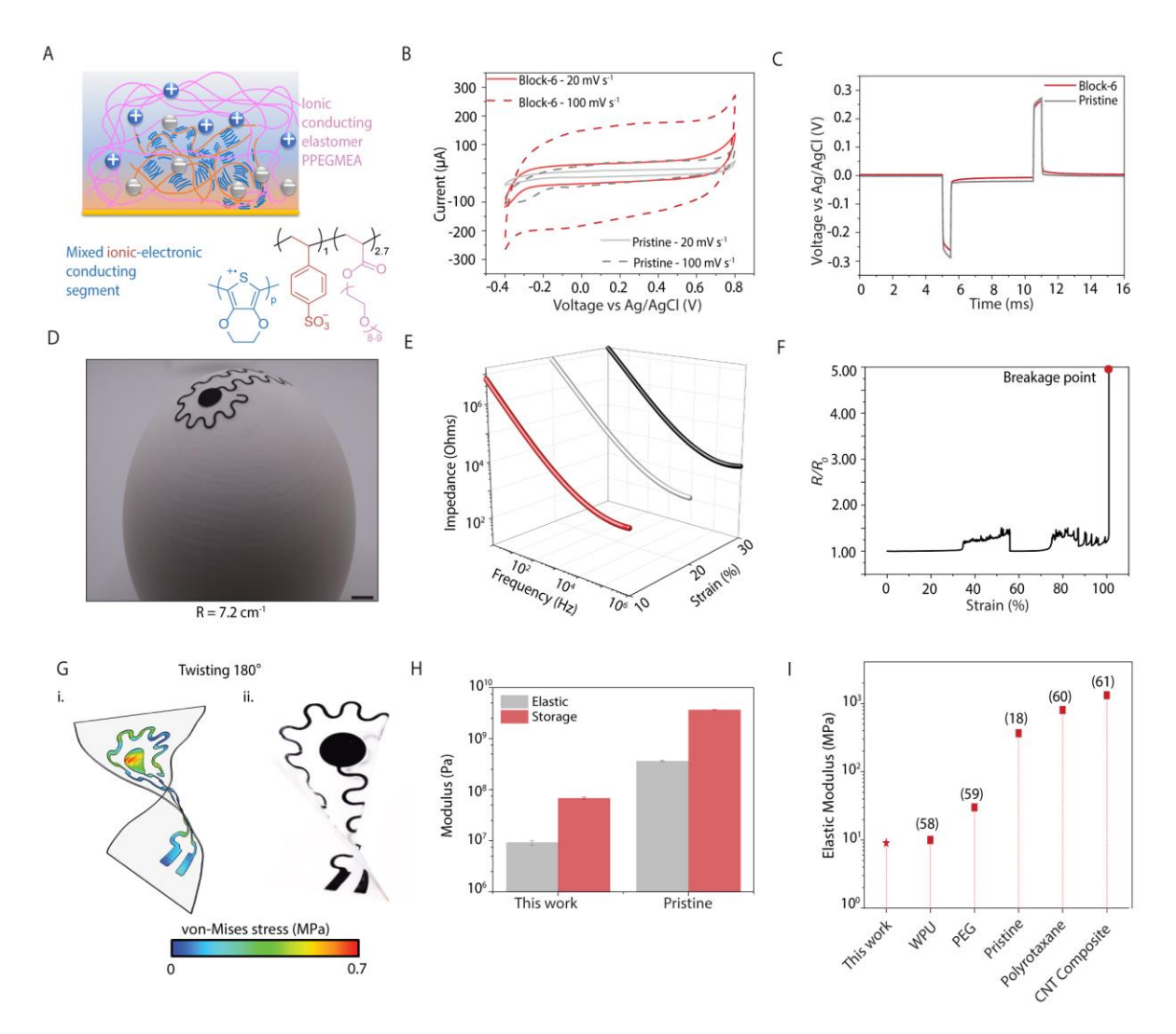


Fig. 2. Electrochemical and electromechanical characterization of conformal electrode. (A) Schematic illustration showing the mixed ionic-electronic conductive segment of PEDOT: PSS and the covalently bound ionic conductive elastomer PPEGMEA segment. (B) Cyclic voltammetry scans of Block-6 and pristine PEDOT: PSS from $20-100 \text{ mV s}^{-1}$ in 20 mV s^{-1} step increments. (C) Comparable voltage build-up during charge injection through the Block-6 and pristine PEDOT: PSS films. (D) Photograph of a concentric Block-6 electrode on a spherical surface. Scale bar is 8 mm. (E) Interfacial impedance of a concentric Block-6 electrode after different strains illustrating the stability of the conformal dry electrode. (F) Change of resistance of Block-6 as a function of strain applied. Fluctuations are due to twisting and buckling until the device is constrained to a unidirectional motion. (G) Finite element analysis (FEA) simulations (i) and photograph of device (ii) after twisting 180° results in low von-Mises stress. (H) Comparison of elastic and storage moduli for Block-6 and pristine PEDOT: PSS, showing copolymerization resulting in increased softness and deformability. (I) Comparison of elastic modulus of Block-6 as used in this work with PEDOT: PSS, as blended with other polymers (18, 58–60), and nanomaterials (61).

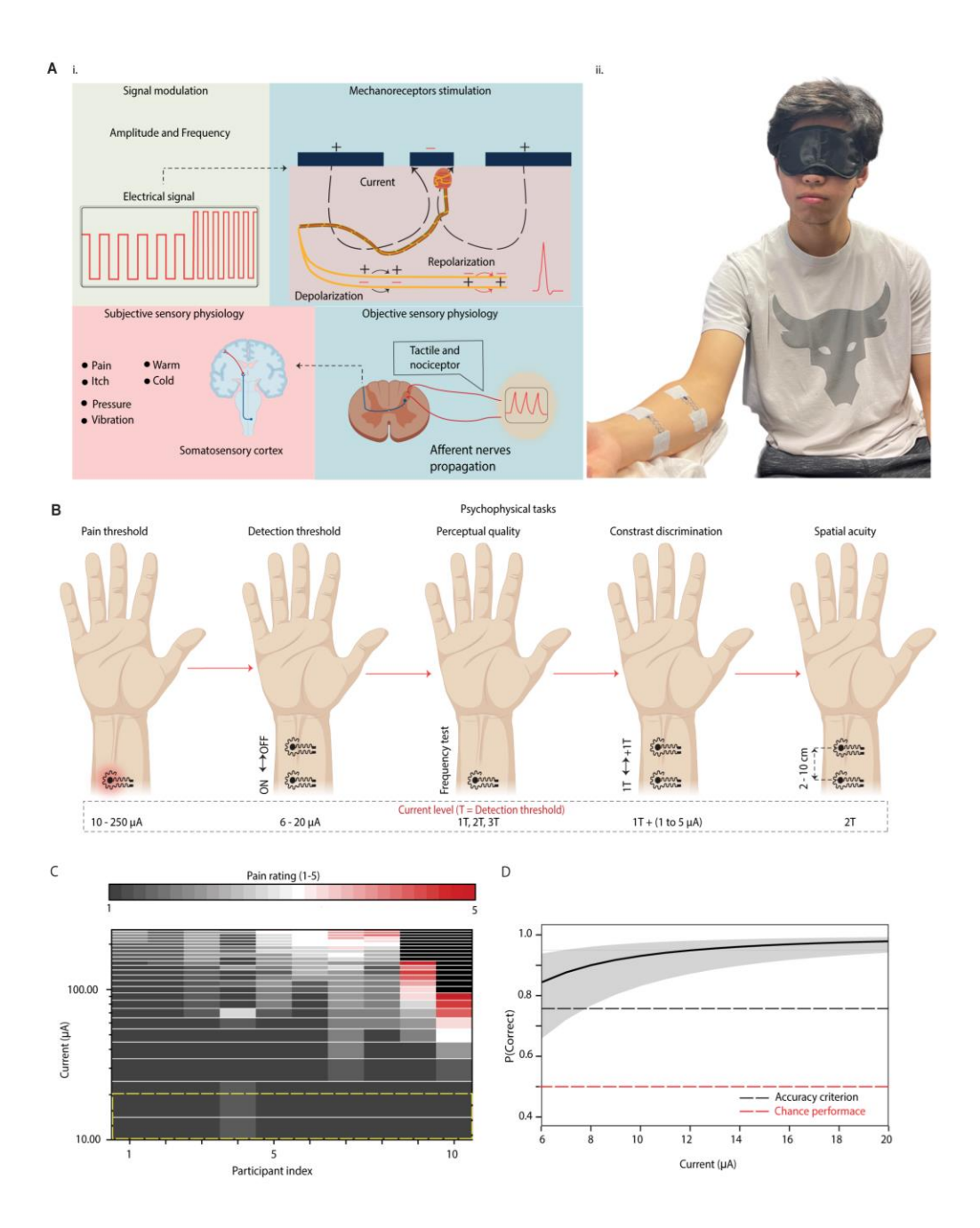


Fig. 3 Experimental setup of psychophysical tasks for electrotactile perception (A) (i) Flow diagram of haptic perception by signal modulation and activation of mechanoreceptors (ii) Participant performing the psychophysical task. (B) Flow diagram of psychophysical tasks performed on the forearm and the current level applied. (C) Heat map of pain threshold (1-5) as a function of current from 10 to 250 μ A, where the yellow dashed box shows the stimulation window used for the detection threshold (n = 639 trials). (D) Participant accuracy (y-axis) in 2-alternative forced choice 2AFC detection task as a function of stimulation current. Red dashed line depicts chance performance. Black dashed line depicts accuracy criterion and red dashed line depicts chance performance. Data are estimated marginal means of generalized linear mixed model (GLMM) fixed effect (black line) and 95% confidence interval on fixed effect (shaded grey ribbon), transformed to response scale with inverse logit function (n = 1280 trials).

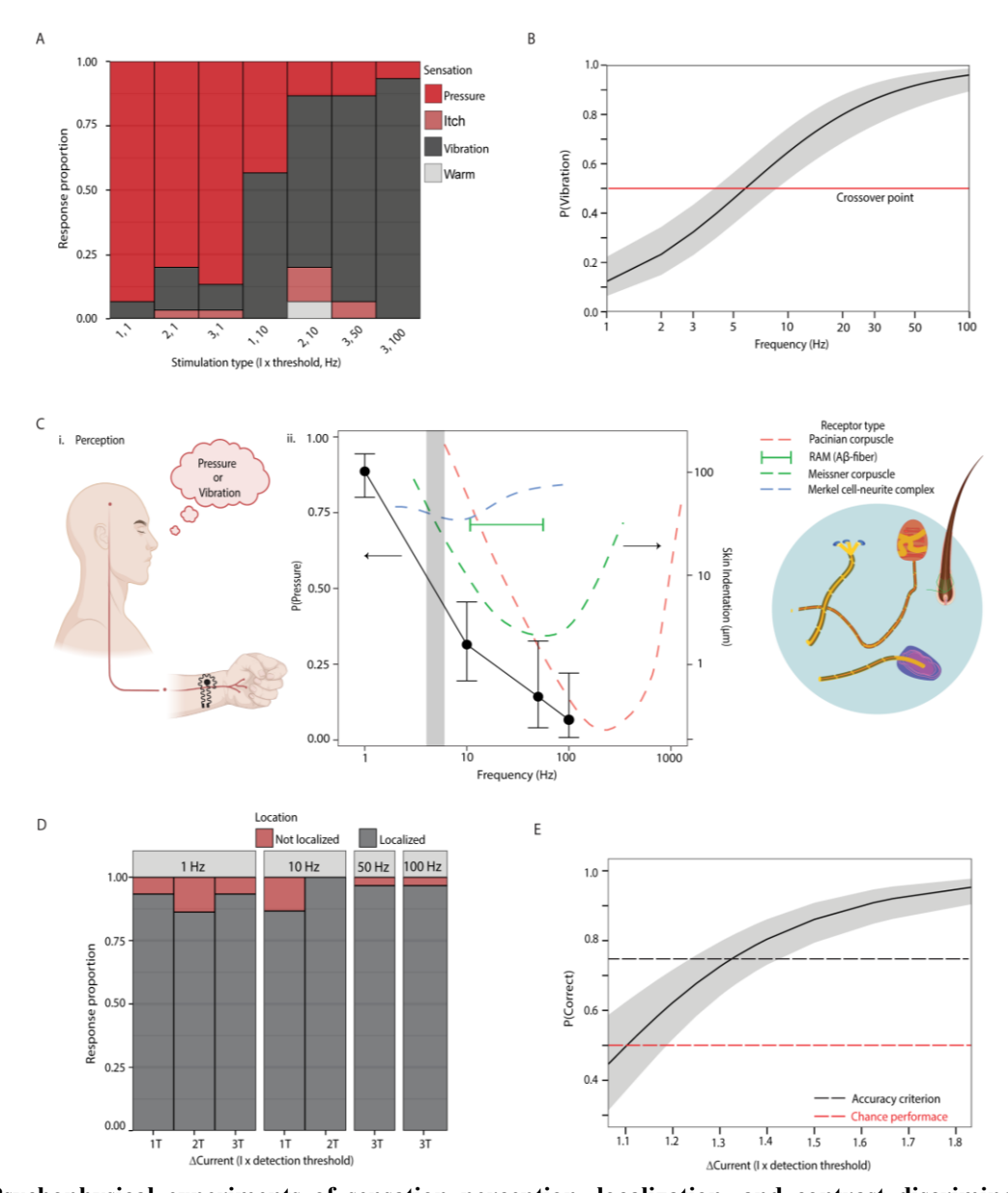


Fig. 4 Psychophysical experiments of sensation perception, localization, and contrast discrimination. (A) Proportion of the time a stimulus is judged as pressure, itch, warm, or vibration (y-axis) as a function of type of stimulation (x-axis). Stimulation type is a combination of stimulation frequency (Hz) and stimulation current (multiple of the participant's detection threshold) (n = 210 trails). (B) Model of the probability of reporting vibration versus pressure (y-axis) as a function of stimulation frequency (x-axis; Hz). Red line depicts crossover point. Data are estimated marginal means of generalized linear mixed models (GLMM) fixed effect (black line) and 95% confidence interval on fixed effect (shaded grey ribbon). (C) (i) Schematic illustration of the participants perceiving different sensations. (ii) Response proportion for pressure normalized by frequency (black line) and compared to receptor temporal sensitivity (red, green, and blue dashed lines). The grey highlight shows the crossover point at ~6 Hz overlaying the sensitivity of Meissner corpuscle and Merkel cells. he green horizontal line shows the range of frequencies for sensitivity to vibration of Aβ-fiber RAMs on hairy skin Error bars are 95% confidence intervals on binomial proportion (Clopper Pearson method), from N=30 participants (200 trials total). Modified with permission from Fig. 1-2 of (62). Copyright © 2007, Springer Science Business Media, LLC, Springer Nature. (D) Participant response to localization as a function of threshold and frequency (n = 210 trials). (E) Participant accuracy (y-axis) in 2AFC discrimination task as a function of difference in stimulation current. Red dashed line depicts chance performance, black dashed line depicts classic accuracy criterion for sensory detection. Data are estimated marginal

10

means of GLMM fixed effect (black line) and 95% confidence interval on fixed effect (shaded grey ribbon) (n = 400 trials).

Materials and Methods

Number-average molecular weight (M_n), weight-average molecular weight (M_w), and dispersity (D) were determined using an Agilent Technologies 1260 Infinity II LC system. The mobile phase was 30% methanol and 70% 0.2 M sodium nitrate (NaNO₃) and 0.01 M monosodium phosphate (NaH₂PO₄) in water at pH 7 (adjusted with concentrated sodium hydroxide, NaOH) at 40 °C at 1 mL min⁻¹. The PL aquagel-OH Mixed-B column was used, calibrated against narrow dispersity PSS standards (purchased from Polymer Standards Service). ¹H nuclear magnetic resonance (NMR) spectra were acquired in deuterium oxide D₂O at room temperature on a Bruker AVANCE III 600 MHz NMR spectrometer fitted with a 1.7 mm triple resonance probe with the z-gradient.

Materials

5

10

15

20

25

30

45

Sodium 4-styrenesulfonate (NaSS), 4,4'-azobis(4-cyanovaleric acid) (ACVA), mol^{-1}), azobis(isobutyronitrile) (AIBN), **PEGMEA** (M_n) 480 4-cyano-4-(phenylcarbonothioylthio)pentanoic acid (the reversible addition fragmentation transfer (RAFT) chain transfer agent), and ethylenedioxythiophene (EDOT) were purchased from Sigma-Aldrich and used without further purification. Distilled water filtered using a Milli-Q purification system was used throughout.

Synthesis of PEDOT:PSS₍₁₎-b-PPEGMEA₍₆₎ (Block-6)

RAFT Polymerization of PSS₍₁₎-b-PPEGMEA₍₆₎ block copolymer

PSS₍₁₎-b-PPEGMEA₍₆₎ was synthesized as previously described (*18*). Briefly, PSS macro-RAFT was synthesized by RAFT polymerization of sodium styrene sulfonate (NaSS) monomers. The RAFT agent was 4-cyano-4-(phenylcarbonothioylthio)pentanoic acid, and the initiator was (4,4'-Azobis(4-cyanovaleric acid)) ACVA. The reaction ratio was 0.2:1:150 initiator:RAFT agent:monomers. The reaction was stopped by exposure to air. PSS macro-RAFT was purified by precipitation in acetone and dried under vacuum to afford a pink powder. Next, to synthesize the PSS-b-PPEGMEA, PSS macro-RAFT, the ACVA initiator and PEGMEA monomers were polymerized via second RAFT polymerization. The reaction ratio was 0.2:1:400 [initiator]:[PSS macro-RAFT agent]:[monomers]. The ¹H NMR of the crude mixtures showed 93% PEGMEA conversion.

Synthesis of PEDOT: PSS₍₁₎-b-PPEGMEA₍₆₎ (Block-6)

PEDOT:PSS(1)-b-PPEGMEA(6) was synthesized as previously reported (18). Briefly, PSS(1)-b-PPEGMEA(X) was dissolved in MiliQ water, at a concentration of 75 mg mL-1 and was acidified by Dowex Marathon C hydrogen form for 18 h. The polymer solution was filtered over a 10 μm filter. Sodium persulfate (1150 mg, 4.83 mmol) and iron trichloride (100 wt % in water, 0.175 mL) were added to the filtrates of 4875 mg of PSS₍₁₎-b-PPEGMEA₍₆₎, 65 mL. The solution was vigorously stirred before the addition of EDOT (500 mg, 3.51 mmol). MiliQ water was added in small portions to prevent gelation. The final volume was 180 mL. The reaction was left to react for 24 hours at room temperature. PEDOT:[PSS₍₁₎-b-PPEGMEA₍₆₎] was purified by stirring over acidic resin (Dowex Marathon C hydrogen form, 17 g) and basic resin (Lewatit MP-62 free base, 11 g) for 6 h, followed by a 10 μm filtration.

Fabrication of the Block-6 film

A custom mold made from Clear V4 resin was 3D-printed (Form 3+) with a thickness of 0.5 mm for drop casting. The mold was sonicated with isopropyl alcohol (IPA), acetone, and deionized (DI) water, sequentially and then dried with nitrogen (N₂) gas. Mold release (Ease Release 200, Mann Release Technologies) was sprayed on the 3D-printed mold and was let to dry at room temperature. Block-6 ink was vigorously stirred and degassed for at least an hour each prior to drop casting. A disposable plastic syringe (1 mL, Henke-Ject) was used to disperse 6.5 mL of the solution. The film was dried on a hot plate covered with a Pyrex tray at 65 °C for 1 hour and 30 min. The film thickness was measured with a profilometer (~20 μm, Bruker Dektak XT stylus). The film was peeled using tweezers and stored in a plastic storage container.

10

15

20

25

30

35

40

5

Psychophysics Procedure and Statistical Analysis

Participants' recruitment and safety protocol assessment

The experimental protocol was approved by the Internal Review Board at the University of California San Diego Human Research Protections Program. Ten healthy volunteers were recruited from the University of California San Diego participated in this study. This sample size fits a pilot study size (14). All steps were taken to ensure a diverse set of participants. The participants had no visible skin cuts or infections in the application area. The participants were blinded for the input of stimulation. Inclusion criteria comprised individuals from a healthy demographic, aged between 18 and 40 years. The age range of 18 to 40 was selected due to the lower likelihood of chronic diseases in this age group. Exclusion criteria included: pregnancy, absence of skin injuries on or near the stimulation sites, rubber or elastomer allergies, highly sensitive skin, presence of pacemakers or other electrical or metal implants in the body, epilepsy or heart conditions, self-reported cancer or neurodegenerative diseases, and allergic reactions to topical moisturizers. We evaluated the safety of our electrodes during stimulation by thermal infrared imaging to detect any joule heating effects (Fig. S31). In addition, we measured the source voltage required to stimulate currents on the finger and the forearm in contrast to recent reports (fig. S32). After assessing safety protocols, our ten human participants were subjected to experiments with the haptic device on the ventral forearm. Biphasic current stimulation is advisable to minimize pain perception and avoid half-cell reactions (45). Quantifying pain thresholds enables us to know if a participant feels noxious for succeeding tasks.

Electrical stimulation and trials protocol

Stimulation parameters

Before placing the electrode on the skin, we wanted to ensure skin condition was similar as possible between different participants because it has a strong influence on the variables, and thus affects the sensation and comfort of stimulation. To remove the insulating layer of the stratum corneum that bears a high impedance of $100 \text{ k}\Omega$, the skin was scrapped gently with 3M Red DotTM Trace Prep and with 70% alcohol prep pad (11). In addition, since the conductive path through the skin is not uniform at the microscopic level due to minute epithelial breaks, we used Q-tips to minimally wet the surface with MiliQ water before placing the electrode (20, 46).

Stimulation was performed with constant current. Constant current is usually used since sweat can build up (20, 47). A symmetric, biphasic, square waveform with 50% duty cycle was used. The

square waveform is preferred due to its ease of implementation and interpretation in electrotactile feedback applications. In addition, they also resulted in a faster depolarization of the nerves axon, which promotes effective stimulation (43). Continuous Biphasic was used since it can prevent skin irritation caused by the transfer of ions within axon membranes and it can also provide a wider range of stimulation parameters and more effectively elicit diverse tactile sensations in lower currents it generates a better spread of current compared to monophasic stimulation (48, 49). Modulation of one or more parameters, such as amplitude or frequency can render different sensations. In general, the pulse width and amplitude may modulate the perceived intensity, whereas the frequency may modulate the perceived sensation (50, 51). For the evaluation of elicited sensations, the frequency below 100 Hz was considered because earlier studies found that low frequency was the most useful range for sensory communication (52). The sensation elicited at 1 Hz and 10 Hz, represented a lower frequency, The sensation elicited at 50 Hz represented a mid-frequency, and the sensation elicited at 100 Hz, represented a higher frequency. The stimulus amplitudes were standardized across participants by using one, two, and three times the detection threshold (DT) of each participant. The stimulation was applied via either the surface electrode to the forearm skin, or to the forehead. A commercial waveform generator and amplifier (BioPac STMISOLA) (fig. S34) were used to generate the studied stimuli. The electrode placement and stimulation setup are illustrated in fig. S33 to S34.

Measurement of pain threshold

5

10

15

45

One pair of electrodes on the stimulation site. Participants rated the sensation of pain on a scale of 1 (not painful at all) to 5 (uncomfortably painful). A scale of 1-5 for pain detection was used since there is no uniform definition of pain (20). We stimulated the user's skin using 10 μA and increased the current amplitude in increments of 10 μA every two seconds, until 250 μA had been reached or until the participant reported an uncomfortably painful sensation (5/5 on the scale). The frequency was set to 1 Hz. This process was repeated three times, with a two-minute break between each trial. We set an a priori exclusion criterion that any participant who reported an uncomfortably painful (5/5 on the scale) sensation in the stimulation range 10 - 50 μA would be excluded from participating in the remainder of the experiment, no participants did so.

Measurement of detection threshold

We measured the detection threshold using a 2-alternative forced choice (2AFC) detection task. Two pairs of electrodes were applied on the stimulation site (either the forehead or forearm). On each trial, only one of the two electrodes was stimulated, and participants were asked on which site they thought they had been stimulated (even if they were unsure, they were required to guess). There was a total of 128 trials per participant: eight trials for each combination of current (8 levels: 6, 8, 10, 12, 14, 16, 18, 20 μA) and stimulation site (2 levels) at a frequency of 1 Hz. The order of trials was randomized within each participant. We chose 16 trials per current level because it conveniently allowed us to operationalize "above detection threshold" using both the classical psychophysical definition (the current at which accuracy exceeded 75%; specifically 13 out of16 trials correct) and the statistical definition (the current at which accuracy was significantly higher than chance on a binomial test; also 13 out of 16 trials correct).

Measurement of spatial acuity

We measured the spatial acuity (two-point discrimination) of the electrotactile current using a 2AFC discrimination task. Two electrode pairs were placed on the ventral side of the forearm, one near the medial epicondyle and the other near the wrist. The center-to-center distance between the inner electrode of the electrode pairs systematically varied from 2 - 10 cm in increments of 2 cm.

Stimulation current was set to twice the participant's detection threshold at a frequency of 1 Hz. On each trial, stimulation was delivered to either one or both electrode pairs, and participants were asked whether they thought they had been stimulated in one versus two places (even if they were unsure, they were required to guess). There was a total of 30 trials per participant: three trials for each level of distance (5 levels: 2, 4, 6, 8, and 10 cm) and stimulation type (2 levels: one versus both positions stimulated). There were five blocks of six trials each: one block for each level of stimulus distance. The order of blocks was randomized within each participant, and the order of trials was randomized within each block.

The perceptual quality of sensation evaluation

5

15

20

25

30

35

40

We measured the perceptual quality of stimulation using a self-report questionnaire. One pair of electrodes was placed on the mid-point of the participant's forearm. We systematically varied the stimulation current and frequency to test perception under a wide range of stimulation parameters as follows: 1x detection threshold, 1 Hz, 1x detection threshold, 10 Hz, 2x detection threshold, 1 Hz, 3x detection threshold, 50 Hz, and3x detection threshold, 100 Hz.

There was a total of 21 trials per participant: three trials for each combination of stimulation parameters (7 levels; see above). The order of presentation was randomized within each participant. On each trial, participants were asked to answer four questions regarding the sensation they felt, the comfort and intensity of stimulation, and the location of the sensation. The questions are described in detail in the Supplementary Information in the section "Evaluation of the perceptual quality of sensation".

Contrast discrimination

We measured sensitivity to differences in current strength using a 2AFC task. Two pairs of stimulating electrodes were placed on the forearm by applying the detection limit current of the participants. On each trial, a different amount of current was delivered to each electrode. One electrode was set to the participant's detection threshold, and the other was set to one of five different current amplitudes (either 1, 2, 3, 4, or 5 μ A higher than the participant's detection threshold). For example, if a participant had a detection threshold of 10 μ A, on a given trial one electrode would deliver 10 μ A and the other would deliver either 11, 12, 13, 14, or 15 μ A. On each trial, the electrode delivering the higher current was varied, and the participant was asked at which electrode they thought the sensation was more intense (even if they were unsure, they were required to guess). There was a total of 40 trials per participant: four for each combination of current (5 levels) and location of higher current (2 levels). The order of trials was randomized within participants.

Statistical Analysis

In general, psychophysical experimental data was fit using mixed effect regression frameworks, generalized linear mixed model (GLMMs; either linear or binomial with logit link function, depending on the dependent variable), which are more powerful than alternatives like t-tests on d-prime because GLMMs account for participants' performance on each trial rather than averaging across trials (53). For each experiment, we fit a GLMM with trial outcome as the dependent variable and subject as random effect; the independent variables were experiment-dependent and are described in detail in each subsection below. GLMMs were fit using the lme4 package in R (54), and participant performance at specific levels of the independent variables was assessed using

estimated marginal means, calculated using the estimated marginal means (emmeans) package in R (55). All p-values reported in the manuscript are from Wald tests on either regression parameters or estimated marginal means (56).

Measurement of detection threshold

5

10

15

20

25

30

35

40

To quantify the effect of stimulation current on detection accuracy, data from the 2-alternative forced choice (2AFC) detection task were fit using a logistic mixed effect regression (GLMM) with fixed effect of log stimulation current, random effect of participant, and dependent variable of trial outcome (correct/incorrect). Overall, participants were significantly more accurate when stimulation current was higher (GLMM fixed effect $\beta_{log(I)} = 1.79$, $SE_{log(\beta_I)} = 0.25$, Wald Z = 7.20, p < 0.001); on average, each 60% increase in stimulation current doubled the odds of detecting the stimulus. Nevertheless, even at the lowest stimulation current used in the study, participants' performance was much higher than chance (estimated marginal mean, $P(correct)_{I=6mA} = 0.84$, 95% CI [0.66,0.94]), and also higher than the 75% accuracy criterion classically used to define the sensory detection threshold (57). Indeed, we conducted Bonferronicorrected Wald Z tests ($\alpha = 0.006$) of the estimated marginal means at all current levels, and participants' accuracy was significantly greater than chance at all eight current levels (all p < 0.001).

Measurement of spatial acuity

To quantify participants' two-point discrimination, data from the 2AFC two-point discrimination task were fit using a logistic mixed effect regression (GLMM) with fixed effect of electrode distance, random effect of participant, and dependent variable of trial outcome (correct/incorrect). Overall, two-point discrimination was significantly higher than chance (GLMM estimated marginal mean, P(correct) = 0.96, SE = 0.01, Wald Z = 10.68, p < 0.001). There was not a significant relationship between electrode distance and two-point discrimination (GLMM fixed effect $\beta_d = 0.07$, $SE_{\beta_d} = 0.11$, Wald Z = 0.62, p = 0.53). This null effect of electrode distance is plausibly a ceiling effect due to the physical constraint of electrode spacing: even at the smallest distance possible for our setup (2 cm), accuracy was 93% (estimated marginal mean; 95% CI [0.88,0.98]), and for 7 of the 10 participants accuracy was 100%. Note that the GLMM model yielded a singular fit with near-zero variance in the random effect (likely because so many participants had near perfect performance), so to verify that this did not influence our interpretation we reran the analysis as a logistic regression with independent variable of separation distance and a dependent variable of trial outcome (such as dropping the random effect from the model). Doing so did not change the result; indeed, the coefficients are the same as reported above (when rounded to two significant digits).

To quantify two-point discrimination at specific distances (as reported in the main manuscript), we conducted Bonferroni-corrected Wald Z tests ($\alpha = 0.01$) of the estimated marginal means. Participants' accuracy was significantly greater than chance at all five distances (all p < 0.001).

The perceptual quality of sensation evaluation

Qualitative sensation was evaluated across all combinations of stimulation frequency and current in the study. Participants predominantly reported the sensation of either pressure or vibration; in fewer than 5% of trials, a different sensation was reported (itchiness or warmth). We classified these trials as outliers and removed from further analysis. To quantify the relationship between stimulation frequency, stimulation current, and reported sensation (vibration versus pressure), data were fit using a logistic mixed effect regression (GLMM) with fixed effects of (log-transformed)

stimulation frequency, (log-transformed) stimulation current, and their interaction, random effect of participant, and dependent variable of reported sensation (vibration versus pressure). Overall, participants were significantly more likely to experience vibration when stimulation frequency was higher (GLMM fixed effect $\beta_{log(f)} = 1.31$, $SE_{\beta_{log(f)}} = 0.33$, Wald Z = 3.96, p < 0.001). On average, increasing the stimulation frequency by 70% doubled the odds of experiencing vibration (versus pressure), and the model predicts that the "crossover" point at which participants first begin to report vibration more often than pressure is $\sim 6Hz$. In contrast to the effect of stimulation frequency, stimulation current did not significantly influence the type of sensation reported by participants (GLMM fixed effect $\beta_{log(I) \times log(f)}$ and $\beta_{log(I)}$ terms; both p > 0.2).

The Intensity rating for changes in stimulation current was assessed. Whereas changes in stimulation frequency produced qualitatively different sensations (pressure versus vibration), changes in stimulation current seem to produce quantitatively different sensations (more versus less intense). To quantify this observation, data were fit using a linear mixed effect regression (LMM) with fixed effects of log stimulation frequency, log stimulation current, and their interaction, random effect of participant, and dependent variable of reported intensity (1-5 scale). Overall, the sensation produced by stronger currents was rated as significantly more intense (LMM fixed effect $\beta_{log(I)} = 0.36$, $SE_{\beta_{log(I)}} = 0.05$, t(176.01) = 3.18, p = 0.002); on average, doubling the stimulation current increased the intensity rating by approximately 0.25 (on the 1-5 scale).

Next, we assessed the amount of discomfort during stimulations. Importantly, all sensations were reported to be between "Very comfortable" and "Neutral" except for a single trial for a single participant (who rated 10 Hz stimulation at detection threshold as "Uncomfortable").

In addition, we assessed the localization of the perceived stimulation. Almost all sensations (93%) were experienced as localized rather than radiating (5%) or referred (1%). To quantify the relationship between stimulation frequency, stimulation current, and reported location, data were fit using a logistic mixed effect regression (GLMM) with fixed effects of log stimulation frequency, log stimulation current, and their interaction, random effect of participant, and dependent variable of reported location (localized/not localized, dummy coded as 1/0). The probability of experiencing a sensation as localized did not significantly depend on frequency or current (GLMM fixed effect $\beta_{log(I) \times log(f)}$ and $\beta_{log(I)}$ terms; both ps > 0.05). Overall, participants experienced the sensations as localized far more often than would be predicted by chance (GLMM estimated marginal mean, P(localized) > 0.99, SE = 0.009, Wald Z = 2.78, p = 0.005).

Contrast Discrimination

5

10

15

20

25

30

35

40

To quantify participants' ability to discriminate between two different stimulation currents, data from the 2AFC discrimination task were fit using a logistic mixed effect regression (GLMM) with fixed effect of difference in (log-scaled) stimulation current, random effect of participant, and dependent variable of trial outcome (correct/incorrect). Overall, participants were significantly more accurate when the two stimulation currents were more different (GLMM fixed effect $\beta_{\Delta\log(I)} = 5.92$, $SE_{\Delta\log(I)} = 1.00$, $Wald\ Z = 5.94$, p < 0.001); on average, each 13% increase in the difference between stimulation currents doubled the odds of detecting the difference. Furthermore, the smallest difference for which P(correct) > 0.75 (specifically, the psychophysical threshold for discrimination) was 1.33 times the detection threshold (as estimated by GLMM estimated marginal mean, $P(correct|\Delta\log(I) = 1.33) = 0.75$).

Commercial Dual Electrodes

For the comparison study, we have used Ag/AgCl electrodes (EL507, BIOPAC Systems, Inc.) with electrode gel (Spectra 360, BIOPAC Systems, Inc.).

Supplementary Materials

5 Supplementary Methods

Figs. S1 to S39

Tables S1 to S3

References (58 - 100)

References and Notes

10

15

20

25

30

35

40

45

- 1. M. Kitagawa, D. Dokko, A. M. Okamura, D. D. Yuh, Effect of sensory substitution on suture-manipulation forces for robotic surgical systems. *J. Thorac. Cardiovasc. Surg* **129**, 151–158 (2005).
- 2. H. J. B. Witteveen, E. A. Droog, J. S. Rietman, P. H. Veltink, Vibro- and electrotactile user feedback on hand opening for myoelectric forearm prostheses. *IEEE. Trans. Biomed. Eng.* **59**, 2219–2226 (2012).
- 3. D. S. Pamungkas, K. Ward, Electro-tactile feedback system to enhance virtual reality experience Electrotactile feedback system to enhance virtual reality experience. *IJCTE* **8**, 465–470 (2016).
- 4. C. V. Keef, L. V. Kayser, S. Tronboll, C. W. Carpenter, N. B. Root, M. Finn, T. F. O'Connor, S. N. Abuhamdieh, D. M. Davies, R. Runser, Y. S. Meng, V. S. Ramachandran, D. J. Lipomi, Virtual Texture Generated Using Elastomeric Conductive Block Copolymer in a Wireless Multimodal Haptic Glove. *Adv. Intell. Syst.* 2 (2020).
- 5. V. Bucciarelli, N. Gozzi, N. Katic, G. Aiello, M. Razzoli, G. Valle, S. Raspopovic, Multiparametric non-linear TENS modulation to integrate intuitive sensory feedback. *J Neural Eng* **20**, 036026 (2023).
- 6. W. Lin, D. Zhang, W. W. Lee, X. Li, Y. Hong, Q. Pan, R. Zhang, G. Peng, H. Z. Tan, Z. Zhang, L. Wei, Z. Yang, Super-resolution wearable electrotactile rendering system. *Sci Adv* **8**, eabp8738 (2022).
- 7. Y. H. Jung, J. H. Kim, J. A. Rogers, Skin-Integrated Vibrohaptic Interfaces for Virtual and Augmented Reality. *Adv Funct Mater* **31**, 2008805 (2021).
- 8. A. Akhtar, J. Sombeck, B. Boyce, T. Bretl, Controlling sensation intensity for electrotactile stimulation in human-machine interfaces. *Sci. Robot.* **3** (2018).
- 9. L. P. Paredes, S. Dosen, F. Rattay, B. Graimann, D. Farina, The impact of the stimulation frequency on closed-loop control with electrotactile feedback. *J Neuroeng Rehabil* 12, 1–16 (2015).
- 10. B. Geng, J. Dong, W. Jensen, S. Dosen, D. Farina, E. N. Kamavuako, Psychophysical Evaluation of Subdermal Electrical Stimulation in Relation to Prosthesis Sensory Feedback. *IEEE Trans. Neural Syst. Rehabilitation Eng.* **26**, 709–715 (2018).
- 11. A. Mazzotta, M. Carlotti, V. Mattoli, Conformable on-skin devices for thermo-electro-tactile stimulation: materials, design, and fabrication. *Mater Adv* **2**, 1787–1820 (2021).
- 12. X. Yu, Z. Xie, Y. Yu, J. Lee, A. Vazquez-Guardado, H. Luan, J. Ruban, X. Ning, A. Akhtar, D. Li, B. Ji, Y. Liu, R. Sun, J. Cao, Q. Huo, Y. Zhong, C. M. Lee, S. Y. Kim, P. Gutruf, C. Zhang, Y. Xue, Q. Guo, A. Chempakasseril, P. Tian, W. Lu, J. Y. Jeong, Y. J. Yu, J. Cornman, C. S. Tan, B. H. Kim, K. H. Lee, X. Feng, Y. Huang, J. A. Rogers, Skin-integrated wireless haptic interfaces for virtual and augmented reality. *Nature* 575, 473–479 (2019).
- 13. C. Pacchierotti, S. Sinclair, M. Solazzi, A. Frisoli, V. Hayward, D. Prattichizzo, Wearable haptic systems for the fingertip and the hand: Taxonomy, review, and perspectives. *ToH* **10**, 580–600 (2017).
- 14. P. Kourtesis, F. Argelaguet, S. Vizcay, M. Marchal, C. Pacchierotti, Electrotactile Feedback Applications for Hand and Arm Interactions: A Systematic Review, Meta-Analysis, and Future Directions. *IEEE Trans Haptics* **15**, 479–496 (2022).
- 15. Y. Luo, M. Reza Abidian, J.-H. Ahn, D. Akinwande, A. M. Andrews, M. Antonietti, Z. Bao, M. Berggren, C. A. Berkey, C. John Bettinger, J. Chen, P. Chen, W. Cheng, X. Cheng, S.-J. Choi, A. Chortos, C. Dagdeviren, R. H. Dauskardt, C. Di, M. D. Dickey, X. Duan, A. Facchetti, Z. Fan, Y. Fang, J. Feng, X. Feng, H. Gao, W. Gao, X. Gong, C. Fei Guo, X. Guo, M. C. Hartel, Z. He, J. S. Ho, Y. Hu, Q. Huang, Y. Huang, F. Huo, M. M. Hussain, A. Javey, U. Jeong, C. Jiang, X. Jiang, J. Kang, D. Karnaushenko, A. Khademhosseini, D.-H. Kim, I.-D. Kim, D. Kireev, L. Kong, C. Lee, N.-E. Lee, P. See Lee, T.-W. Lee, F.

- Li, J. Li, C. Liang, C. Teck Lim, Y. Lin, D. J. Lipomi, J. Liu, K. Liu, N. Liu, R. Liu, Y. Liu, Y. Liu, Z. Liu, Z. Liu, X. Jun Loh, N. Lu, Z. Lv, S. Magdassi, G. G. Malliaras, N. Matsuhisa, A. Nathan, S. Niu, J. Pan, C. Pang, Q. Pei, H. Peng, D. Qi, H. Ren, J. A. Rogers, A. Rowe, O. G. Schmidt, T. Sekitani, D.-G. Seo, G. Shen, X. Sheng, Q. Shi, T. Someya, Y. Song, E. Stavrinidou, M. Su, X. Sun, K. Takei, X.-M. Tao, B. C. K. Tee, A. Voon-Yew Thean, T. Quang Trung, C. Wan, H. Wang, J. Wang, M. Wang, S. Wang, T. Wang, Z. Lin Wang, P. S. Weiss, H. Wen, S. Xu, T. Xu, H. Yan, X. Yan, H. Yang, L. Yang, S. Yang, L. Yin, C. Yu, G. Yu, J. Yu, S.-H. Yu, X. Yu, E. Zamburg, H. Zhang, X. Zhang, X. Zhang, X. Zhang, Y. Zhang, Y. Zhang, S. Zhao, X. Zhao, Y. Zheng, Y.-Q. Zheng, Z. Zheng, T. Zhou, B. Zhu, M. Zhu, R. Zhu, Y. Zhu, Y. Zhu, G. Zou, X. Chen, Technology Roadmap for Flexible Sensors. *ACS Nano* 17, 5211–5295 (2023).
- 16. E. L. Graczyk, M. A. Schiefer, H. P. Saal, B. P. Delhaye, S. J. Bensmaia, D. J. Tyler, The neural basis of perceived intensity in natural and artificial touch. *Sci. Transl. Med.* **8** (2016).

15

20

25

35

40

- 17. B. Stephens-Fripp, R. Mutlu, G. Alici, A Comparison between Separated Electrodes and Concentric Electrodes for Electrotactile Stimulation. *IEEE Trans. Med. Robot* **3**, 241–252 (2021).
- 18. R. Blau, A. X. Chen, B. Polat, L. L. Becerra, R. Runser, B. Zamanimeymian, K. Choudhary, D. J. Lipomi, Intrinsically Stretchable Block Copolymer Based on PEDOT:PSS for Improved Performance in Bioelectronic Applications. *ACS Appl Mater Interfaces* 14, 4823–4835 (2022).
 - 19. L. V. Kayser, D. J. Lipomi, Stretchable Conductive Polymers and Composites Based on PEDOT and PEDOT:PSS. *Advanced Materials* **31** (2019).
 - 20. K. A. Kaczmarek, J. G. Webster, P. Bach-y-Rita, W. J. Tompkins, Electrotactile and Vibrotactile Displays for Sensory Substitution Systems. *IEEE Trans Biomed Eng* **38**, 1–16 (1991).
 - 21. C. Lim, Y. J. Hong, J. Jung, Y. Shin, S. H. Sunwoo, S. Baik, O. K. Park, S. H. Choi, T. Hyeon, J. H. Kim, S. Lee, D. H. Kim, Tissue-like skin-device interface for wearable bioelectronics by using ultrasoft, mass-permeable, and low-impedance hydrogels. *Sci Adv* 7 (2021).
 - 22. G. Corniani, H. P. Saal, Tactile innervation densities across the whole body. *J Neurophysiol* **124**, 1229–1240 (2020).
 - 23. W. Wang, Y. Jiang, D. Zhong, Z. Zhang, S. Choudhury, J. C. Lai, H. Gong, S. Niu, X. Yan, Y. Zheng, C. C. Shih, R. Ning, Q. Lin, D. Li, Y. H. Kim, J. Kim, Y. X. Wang, C. Zhao, C. Xu, X. Ji, Y. Nishio, H. Lyu, J. B. H. Tok, Z. Bao, Neuromorphic sensorimotor loop embodied by monolithically integrated, low-voltage, soft e-skin. *Science* 380, 735–742 (2023).
- 24. E. Losanno, M. Mender, C. Chestek, S. Shokur, S. Micera, Neurotechnologies to restore hand functions. *Nature Reviews Bioengineering* **1**, 390–407 (2023).
 - 25. R. K. Ray, P. Patel, M. Manivannan, Reduction of electrotactile perception threshold using subthreshold vibrotactile stimuli. *Displays* **69**, 102056 (2021).
 - 26. G. Alon, G. Kantor, H. S. Ho, Effects of Electrode Size on Basic Excitatory Responses and on Selected Stimulus Parameters. https://doi.org/10.2519/jospt.1994.20.1.29 20, 29–35 (1994).
 - 27. H. Yuk, B. Lu, X. Zhao, Hydrogel bioelectronics. Chem. Soc. Rev 48, 1642–1667 (2019).
 - 28. K. Tybrandt, I. V Zozoulenko, M. Berggren, Chemical potential-electric double layer coupling in conjugated polymer-polyelectrolyte blends. (2017).
 - 29. B. D. Paulsen, K. Tybrandt, E. Stavrinidou, J. Rivnay, Organic mixed ionic–electronic conductors. *Nat Mater* **19**, 13–26 (2020).
 - A. V Volkov, K. Wijeratne, E. Mitraka, U. Ail, D. Zhao, K. Tybrandt, J. W. Andreasen, M. Berggren, X. Crispin, I. V Zozoulenko, Understanding the Capacitance of PEDOT:PSS. *Adv Funct Mater* 27, 1700329–1700329 (2017).
 - 31. R. Vatsyayan, S. A. Dayeh, A universal model of electrochemical safety limits in vivo for electrophysiological stimulation. *Front Neurosci* **16**, 972252 (2022).
 - 32. D.-H. Kim, N. Lu, R. Ma, Y.-S. Kim, R.-H. Kim, S. Wang, J. Wu, S. M. Won, H. Tao, A. Islam, K. J. Yu, T.-I. Kim, R. Chowdhury, M. Ying, L. Xu, M. Li, H.-J. Chung, H. Keum, M. Mccormick, P. Liu, Y.-W. Zhang, F. G. Omenetto, Y. Huang, T. Coleman, J. A. Rogers, Epidermal Electronics. *Science* (1979) 333, 838–843 (2011).
- 50 33. C. Ruisheng Guo, Y. Yu, Z. Xie, X. Liu, X. Zhou, Y. Gao, Z. Liu, F. Zhou, Y. Yang, Z. Zheng, R. Guo, F. Zhou, Y. Yu, Z. Xie, X. Liu, X. Zhou, Y. Gao, Z. Liu, Z. J. Zheng, Y. Yang, Matrix-Assisted Catalytic Printing for the Fabrication of Multiscale, Flexible, Foldable, and Stretchable Metal Conductors. *Advanced Materials* 25, 3343–3350 (2013).
- H. Song, G. Luo, Z. Ji, R. Bo, Z. Xue, D. Yan, F. Zhang, K. Bai, J. Liu, X. Cheng, W. Pang, Z. Shen, Y.
 Zhang, Highly-integrated, miniaturized, stretchable electronic systems based on stacked multilayer network materials. *Sci Adv* 8, 3785 (2022).

Submitted Manuscript: Confidential Template revised November 2022

- 35. M. Moroni, M. R. Servin-Vences, R. Fleischer, O. Sánchez-Carranza, G. R. Lewin, Voltage gating of mechanosensitive PIEZO channels. *Nature Communications* 2018 9:1 9, 1–15 (2018).
- 36. D. R. Mcneal, Analysis of a Model for Excitation of Myelinated Nerve. *IEEE Trans Biomed Eng* (1976).
- 37. Å. B. Vallbo, Sensations evoked from the glabrous skin of the human hand by electrical stimulation of unitary mechanosensitive afferents. *Brain Res* **215**, 359–363 (1981).

5

10

15

20

45

50

- 38. D. Purves, "Overview Cutaneous and Subcutaneous Somatic Sensory Receptors" in *Neuroscience*, Purves Dale, Ed. (Sinauer Associates, 3rd edition., 2004), pp. 189–208.
- 39. S. P. McKee, L. Welch, Sequential recruitment in the discrimination of velocity. *Journal of the Optical Society of America A, Vol. 2, Issue 2, pp. 243-251* **2**, 243–251 (1985).
- 40. A. Ikoma, H. Handwerker, Y. Miyachi, M. Schmelz, Electrically evoked itch in humans. *Pain* **113**, 148–154 (2005).
 - 41. Y. Huang, K. Yao, J. Li, D. Li, H. Jia, Y. Liu, C. K. Yiu, W. Park, X. Yu, Recent advances in multi-mode haptic feedback technologies towards wearable interfaces. *Materials Today Physics* **22**, 100602 (2022).
 - 42. I. Birznieks, S. McIntyre, H. M. Nilsson, S. S. Nagi, V. G. Macefield, D. A. Mahns, R. M. Vickery, Tactile sensory channels over-ruled by frequency decoding system that utilizes spike pattern regardless of receptor type. *Elife* **8** (2019).
 - 43. C. Pasluosta, P. Kiele, T. Stieglitz, Paradigms for restoration of somatosensory feedback via stimulation of the peripheral nervous system. *Clinical Neurophysiology* **129**, 851–862 (2018).
 - 44. M. Solomonow, J. Lyman, A. Freedy, Electrotactile Two-Point Discrimination as a Function of Frequency, Body Site, katerality, and Stimulation Codes 1'2. *Ann Biomed Eng* **5**, 47–60 (1977).
 - 45. S. Mottaghi, N. Afshari, O. Buchholz, S. Liebana, U. G. Hofmann, Modular Current Stimulation System for Pre-clinical Studies. *Front Neurosci* **14**, 408 (2020).
 - 46. A. Y. J. Szeto, F. A. Saunders, Electrocutaneous Stimulation for Sensory Communication in Rehabilitation Engineering. *IEEE Trans Biomed Eng* **BME-29**, 300–308 (1982).
- J. L. Mason, N. Mackay, Pain Sensations Associated with Electrocutaneous Stimulation. *IEEE Trans Biomed Eng* **BME-23**, 405–409 (1976).
 - 48. F. A. Lenz, M. Seike, R. T. Richardson, Y. C. Lin, F. H. Baker, I. Khoja, C. J. Jaeger, R. H. Gracely, Thermal and pain sensations evoked by microstimulation in the area of human ventrocaudal nucleus. https://doi.org/10.1152/jn.1993.70.1.200 70, 200–210 (1993).
- 30 49. C. W. Pamungkas Daniel S, Overview Electrotactile Feedback for Enhancing Human Computer Interface. *JournaJournal of Physics: Conference Series*, doi: 10.1088/1742-6596/1007/1/012001 (2018).
 - 50. D. J. Djozic, D. Bojanic, G. Krajoski, N. Popov, V. Ilic, Psychophysical characteristics of electrotactile stimulation: The impact of changes in stimulation pulse width and frequency on human perception. 2015 IEEE 15th International Conference on Bioinformatics and Bioengineering (BIBE), 1–5 (2015).
- 51. K. A. Kaczmarek, M. E. Tyler, A. J. Brisben, K. O. Johnson, The afferent neural response to electrotactile stimuli: Preliminary results. *IEEE Transactions on Rehabilitation Engineering* **8**, 268–270 (2000).
 - 52. A. Y. J. Szeto, J. Lyman, R. E. Prior, Electrocutaneous Pulse Rate and Pulse Width Psychometric Functions for Sensory Communications. *Human Factors: The Journal of the Human Factors and Ergonomics Society* **21**, 241–249 (1979).
- 40 53. A. Moscatelli, M. Mezzetti, F. Lacquaniti, Modeling psychophysical data at the population-level: The generalized linear mixed model. *J Vis* **12**, 26–26 (2012).
 - 54. D. Bates, M. Mächler, B. M. Bolker, S. C. Walker, Fitting Linear Mixed-Effects Models Using Ime4. *J Stat Softw* **67**, 1–48 (2015).
 - 55. S. R. Searle, F. M. Speed, G. A. Milliken, R. Searle, Population Marginal Means in the Linear Model: An Alternative to Least Squares Means Population Marginal Means in the Linear Model: An Alternative to Least Squares Means s. *Am Stat* 34, 216–221 (1980).
 - 56. A. Wald, Tests of statistical hypotheses concerning several parameters when the number of observations is large. *Trans Am Math Soc* **54**, 426–482 (1943).
 - 57. S. P. Mckee, S. A. Klein, D. Y. Teller, Statistical properties of forced-choice psychometric functions: Implications of probit analysis. *Percept Psychophys* **37**, 286–298 (1985).
 - 58. N. Kim, S. Lienemann, I. Petsagkourakis, D. Alemu Mengistie, S. Kee, T. Ederth, V. Gueskine, P. Leclère, R. Lazzaroni, X. Crispin, K. Tybrandt, Elastic conducting polymer composites in thermoelectric modules. *Nature Communications* 2020 11:1 11, 1–10 (2020).
 - 59. Y. Li, X. Li, S. Zhang, L. Liu, N. Hamad, S. R. Bobbara, D. Pasini, F. Cicoira, Autonomic Self-Healing of PEDOT:PSS Achieved Via Polyethylene Glycol Addition. *Adv Funct Mater* **30**, 2002853 (2020).
 - 60. Y. Jiang, Z. Zhang, Y. X. Wang, D. Li, C. T. Coen, E. Hwaun, G. Chen, H. C. Wu, D. Zhong, S. Niu, W. Wang, A. Saberi, J. C. Lai, Y. Wu, Y. Wang, A. A. Trotsyuk, K. Y. Loh, C. C. Shih, W. Xu, K. Liang, K.

Submitted Manuscript: Confidential Template revised November 2022

- Zhang, Y. Bai, G. Gurusankar, W. Hu, W. Jia, Z. Cheng, R. H. Dauskardt, G. C. Gurtner, J. B. H. Tok, K. Deisseroth, I. Soltesz, Z. Bao, Topological supramolecular network enabled high-conductivity, stretchable organic bioelectronics. *Science* (1979) 375, 1411–1417 (2022).
- 61. C. Xu, S. Yang, P. Li, H. Wang, H. Li, Z. Liu, Wet-spun PEDOT:PSS/CNT composite fibers for wearable thermoelectric energy harvesting. *Composites Communications* **32**, 101179 (2022).
- 62. A. W. Roe, R. M. Friedman, L. M. Chen, Multiple representation in primate SI: A view from a window on the brain. *Handbook of Neurochemistry and Molecular Neurobiology: Sensory Neurochemistry*, 1–16 (2007).
- 63. W. Humphrey, A. Dalke, K. Schulten, VMD: Visual molecular dynamics. *J Mol Graph* 14, 33–38 (1996).
- 10 64. S. L. Mayo, B. D. Olafson, W. A. Goddard, DREIDING: A generic force field for molecular simulations. *Journal of Physical Chemistry* **94**, 8897–8909 (1990).

5

15

20

35

40

45

50

- 65. A. P. Thompson, H. M. Aktulga, R. Berger, D. S. Bolintineanu, W. M. Brown, P. S. Crozier, P. J. in 't Veld, A. Kohlmeyer, S. G. Moore, T. D. Nguyen, R. Shan, M. J. Stevens, J. Tranchida, C. Trott, S. J. Plimpton, LAMMPS a flexible simulation tool for particle-based materials modeling at the atomic, meso, and continuum scales. *Comput Phys Commun* 271, 108171 (2022).
- 66. T. Shire, K. J. Hanley, K. Stratford, DEM simulations of polydisperse media: efficient contact detection applied to investigate the quasi-static limit. *Comput Part Mech* **8**, 653–663 (2021).
- 67. P. J. in 't Veld, S. J. Plimpton, G. S. Grest, Accurate and efficient methods for modeling colloidal mixtures in an explicit solvent using molecular dynamics. *Comput Phys Commun* **179**, 320–329 (2008).
- 68. A. Kausar, Fabrication and Characteristics of Poly(benzimidazole/fluoro/ether/siloxane/amide)/Sulfonated Polystyrene/Silica Nanoparticle-Based Proton Exchange Membranes Doped With Phosphoric Acid. http://dx.doi.org/10.1080/00914037.2014.936589 64, 184–191 (2014).
 - 69. B. T. N. C. Andrade, A. C. D. S. Bezerra, C. R. Calado, Adding value to polystyrene waste by chemically transforming it into sulfonated polystyrene. *Matéria (Rio de Janeiro)* **24**, e12417 (2019).
- 25 70. B. W. Chieng, N. A. Ibrahim, W. M. Z. W. Yunus, M. Z. Hussein, Poly(lactic acid)/Poly(ethylene glycol) Polymer Nanocomposites: Effects of Graphene Nanoplatelets. *Polymers 2014, Vol. 6, Pages 93-104* **6**, 93–104 (2013).
 - 71. N. S. Vrandečić, M. Erceg, M. Jakić, I. Klarić, Kinetic analysis of thermal degradation of poly(ethylene glycol) and poly(ethylene oxide)s of different molecular weight. *Thermochim Acta* **498**, 71–80 (2010).
- W. W. Chiu, J. Travaš-Sejdić, R. P. Cooney, G. A. Bowmaker, Studies of dopant effects in poly(3,4-ethylenedioxythiophene) using Raman spectroscopy. *Journal of Raman Spectroscopy* **37**, 1354–1361 (2006).
 - 73. S. Nešpůrek, P. Kuberský, R. Polanský, M. Trchová, J. Šebera, V. Sychrovský, Raman spectroscopy and DFT calculations of PEDOT:PSS in a dipolar field. *Physical Chemistry Chemical Physics* **24**, 541–550 (2021)
 - 74. R. Wang, Y. Wang, C. Wu, T. Zhai, J. Yang, B. Sun, S. Duhm, N. Koch, Direct Observation of Conductive Polymer Induced Inversion Layer in n-Si and Correlation to Solar Cell Performance. *Adv Funct Mater* **30**, 1903440 (2020).
 - 75. S. Ne Perrot, F. Pawula, S. Pechev, G. Hadziioannou, G. Fleury, PEDOT:Tos electronic and thermoelectric properties: lessons from two polymerization processes †. *J. Mater. Chem. C* **9**, 7417–7425 (2021).
 - 76. C. V Amanchukwu, M. Gauthier, T. P. Batcho, C. Symister, Y. Shao-Horn, J. M. D'arcy, P. T. Hammond, Evaluation and Stability of PEDOT Polymer Electrodes for Li-O 2 Batteries. *J. Phys. Chem. Lett* 7, 19 (2016).
 - 77. S. Bhatt, J. Pulpytel, M. Mirshahi, F. Arefi-Khonsari, Catalyst-free plasma-assisted copolymerization of poly(ε-caprolactone) -poly(ethylene glycol) for biomedical applications. *ACS Macro Lett* 1, 764–767 (2012).
 - 78. L. H. Rong, X. Cheng, J. Ge, O. K. Krebs, J. R. Capadona, E. B. Caldona, R. C. Advincula, SI-PET-RAFT Polymerization via Electrodeposited Macroinitiator Thin Films: Toward Biomedical and Sensing Applications. *ACS Appl Polym Mater* 4, 6449–6457 (2022).
 - 79. G. M. Veith, M. Doucet, R. L. Sacci, B. Vacaliuc, J. K. Baldwin, J. F. Browning, Determination of the Solid Electrolyte Interphase Structure Grown on a Silicon Electrode Using a Fluoroethylene Carbonate Additive OPEN. doi: 10.1038/s41598-017-06555-8 (2017).
 - 80. L. P. Bütikofer R, Electrocutaneous nerve stimulation--I: model and experiment. *IEEE Trans Biomed Eng* **6**, 526–531 (1978).
 - 81. T. Edmond, A. Laps, A. L. Case, N. O'Hara, J. M. Abzug, Normal Ranges of Upper Extremity Length, Circumference, and Rate of Growth in the Pediatric Population. *Hand* **15**, 713–721 (2020).
 - 82. G. Li, S. Wang, Y. Y. Duan, Towards gel-free electrodes: A systematic study of electrode-skin impedance. *Sens Actuators B Chem* **241**, 1244–1255 (2017).

- 83. I. J. Jossinet, A. Lackermeier, F. Risacher, Factors affecting electrode-gel-skin interface impedance in electrical impedance tomography. *Biol. Eng. & Comput* **34**, 397–408 (1996).
- 84. Geoffrey K. Reeves, H. Barry Harrison, Obtaining the specific contact resistance from transmission line model measurements. *IEEE Electron Device Letters* **3**, 111–113 (1982).
- 85. Y. Park, C. K. Franz, H. Ryu, H. Luan, K. Y. Cotton, J. Uk Kim, T. S. Chung, S. Zhao, A. Vazquez-Guardado, D. Som Yang, K. Li, R. Avila, J. K. Phillips, M. J. Quezada, H. Jang, S. Soo Kwak, S. Min Won, K. Kwon, H. Jeong, A. J. Bandodkar, M. Han, H. Zhao, G. R. Osher, H. Wang, K. Lee, Y. Zhang, Y. Huang, J. D. Finan, J. A. Rogers, Three-dimensional, multifunctional neural interfaces for cortical spheroids and engineered assembloids. *Sci. Adv* 7, 9153–9170 (2021).
- 10 86. A. Wiranata, S. Maeda, Implementation of SYLGARD 184 for powder-based dielectric elastomer actuators. *SEATUC journal of science and engineering* **1**, 14–19 (2020).
 - 87. M. Rahimi, F. Jiang, Y. Shen, Spatiotemporal Identification of Moving Patterns on a Fingertip-based Electro-Tactile Display Array. *TechRxiv*, 1–10 (2020).
 - 88. S. E. Root, C. W. Carpenter, L. V. Kayser, D. Rodriquez, D. M. Davies, S. Wang, S. T. M. Tan, Y. S. Meng, D. J. Lipomi, Ionotactile Stimulation: Nonvolatile Ionic Gels for Human-Machine Interfaces. *ACS Omega* 3, 662–666 (2018).
 - 89. H. Kajimoto, Electrotactile Display with Real-Time Impedance Feedback Using Pulse Width Modulation. *IEEE Trans Haptics* **5**, 184–188 (2012).
 - 90. H. Kajimoto, N. Kawakami, S. Tachi, "Electro-Tactile Display with Tactile Primary Color Approach" in *Int. Conf. on Intelligent Robots and Systems* (2004).
 - 91. S. Gabriel, R. W. Lau, C. Gabriel, The dielectric properties of biological tissues: II. Measurements in the frequency range 10 Hz to 20 GHz. *Physics in Medicine* **41**, 2251–2269 (1996).
 - 92. Y. E. Shuan, K. Zhu, P. Li, S. Xiaohong, Neural Firing Mechanism Underlying Two-Electrode Discrimination by 3D Transcutaneous Electrical Nerve Stimulation Computational Model. *Jiao Tong Univ.* (Sci.) 24, 716–722 (2019).
 - 93. Koch Christof, "The Hodgkin and Huxley Model of Action Potential Generation" in *Biophysics of Computation*, Christof Koch, Ed. (Oxford university press, 2004), pp. 139–174.
 - 94. Franceschi Marta, Seminara Lucia, Dosen Strahinja, Strbac Matija, Valle Maurizio, Farina Dario, A System for Electrotactile Feedback Using Electronic Skin and Flexible Matrix Electrodes: Experimental Evaluation. *IEEE Transections on Haptics* **10**, 162–172 (2017).
 - 95. B. Geng, K. Yoshida, L. Petrini, W. Jensen, Evaluation of sensation evoked by electrocutaneous stimulation on forearm in nondisabled subjects. *J Rehabil Res Dev* **49**, 297–308 (2012).
 - 96. T. Tashiro, The perceptual properties of electrocutaneous stimulation: Sensory quality, subjective intensity, sand intensity-duration relation. *Percept Psychophys* **30**, 579–586 (1981).
- 97. M. Perović, M. Stevanović, T. Jevtić, M. Štrbac, G. Bijelić, Č. Vučetić, L. Popović-Maneski, D. B. Popović, Electrical stimulation of the forearm: A method for transmitting sensory signals from the artificial hand to the brain. *Journal of Automatic Control* 21, 13–18 (2013).
 - 98. V. Yem, H. Kajimoto, Comparative Evaluation of Tactile Sensation by Electrical and Mechanical Stimulation. *IEEE Trans Haptics* **10**, 130–134 (2017).
- 40 99. K. Choi, P. Kim, K. S. Kim, S. Kim, Mixed-modality stimulation to evoke two modalities simultaneously in one channel for electrocutaneous sensory feedback. *IEEE Transactions on Neural Systems and Rehabilitation Engineering* **25**, 2258–2269 (2017).
 - 100. H. Kajimoto, N. Kawakami, S. Tachi, "Psychophysical evaluation of receptor selectivity in electro-tactile display" in *SICE System Integration Division Annual Conference 2002* (2002), p. 418.

Acknowledgments

5

15

20

25

30

45

50

This work was supported by the National Science Foundation Disability and Rehabilitation Engineering program under grant no. CBET-2223566. Aspects of the development of the conductive block copolymer were supported by Air Force Office of Scientific Research (AFOSR) grant no. FA9550-19-1-0278. R.B. acknowledges that this project has received funding from the European Union's Horizon 2020 research and innovation programme under the Marie Skłodowska-Curie Grant Agreement No 898571. A.A. acknowledges financial support from the Kuwait Foundation for the Advancement of Sciences (KFAS). A.X.C. acknowledges financial support from the UC President's Dissertation Year Fellowship. L.L.B. acknowledges support from

the National Science Foundation Graduate Research Fellowship (NSF GRFP) under grant no. DGE-2038238 and funding from the Achievement Rewards for College Scientists (ARCS) Foundation. N.R. and R.R. acknowledge financial support from the Dutch Research Council (NWO) under Grant 406.21.GO.021. The authors thank Prof. Jinhye Bae and Lisa Tang for their support with optical microscopy measurements, as well as Prof. Nicholas Boechler for helpful discussions. We would like to thank Prof. Padmini Rangamani and Mayte Quintana for their guidance with computational biophysics. The authors thank Dr. Ich C. Tran. Ph.D. for his help with XPS analysis, where work was performed using instrumentation funded in part by the National Science Foundation Major Research Instrumentation Program under grant no. CHE-1338173. S.M.R. and S.A.D. were partially supported by the National Institutes of Health primarily through Award No. NIBIB DP2-EB029757 (to S.A.D.) and in part by the BRAIN® Initiative NIH grants R01NS123655 (to S.A.D.), UG3NS123723 (to S.A.D.). The authors acknowledge the use of facilities and instrumentation at the UC Irvine Materials Research Institute (IMRI), which is supported in part by the National Science Foundation through the UC Irvine Materials Research Science and Engineering Center (DMR-2011967). This work was performed in part at the San Diego Nanotechnology Infrastructure (SDNI), a member of the National Nanotechnology Coordinated Infrastructure, which is supported by the National Science Foundation (grant ECCS-1542148). All human participants testing were conducted in accordance with the ethical guidelines with the approval of the Institutional Review Board (#805425) of the University of California, San Diego. Elements of Figures 3A, 3B, and 4C were illustrated by BioRender.com.

Funding:

5

10

15

20

25

30

35

40

National Science Foundation (grant CBET-2223566)

Author contributions:

Conceptualization: RB, AA, DJL

Methodology: RB, AA, NR, AXC, RR, YQ, TR, TK, AN, JC, SE, LLB, SMR, SAD

Investigation: RB, AA, NR

Visualization: RB, AA, NR, TR

Funding acquisition: DJL

Project administration: RB, AA, DJL

Supervision: DJL

Writing – original draft: RB, AA, NR

Writing – review & editing: RB, AA, NR, AXC, DPF, DJL

Competing interests: S.A.D. has competing interests that are not related to this work including equity in Cortical Sciences Inc. that concerns with the commercialization of brain recording and stimulation electrodes, and as a paid consultant to MaXentric Technologies.

Data and materials availability: All data are available in the main text or the supplementary materials. The code to generate statistics and visualizations is available at DOI: 10.5281/zenodo.11177411.

Submitted Manuscript: Confidential Template revised November 2022